
GUIDED INTERPOLATION FOR ADVERSARIAL TRAINING

Chen Chen^{1*}, Jingfeng Zhang^{2*}, Xilie Xu³, Tianlei Hu¹, Gang Niu², Gang Chen^{1†}, Masashi Sugiyama^{2,4}

¹ College of Computer Science and Technology, Zhejiang University

² RIKEN Center for Advanced Intelligence Project (AIP)

³ Taishan College, Shandong University

⁴ The University of Tokyo

ABSTRACT

To enhance *adversarial robustness*, *adversarial training* learns deep neural networks on the *adversarial variants* generated by their natural data. However, as the training progresses, the training data becomes less and less *attackable*, undermining the robustness enhancement. A straightforward remedy is to incorporate more training data, but sometimes incurring an unaffordable cost. In this paper, to mitigate this issue, we propose the *guided interpolation framework* (GIF): in each epoch, the GIF employs the previous epoch’s meta information to guide the data’s interpolation. Compared with the vanilla *mixup*, the GIF can provide a higher ratio of attackable data, which is beneficial to the robustness enhancement; it meanwhile mitigates the model’s linear behavior between classes, where the linear behavior is favorable to *standard training for generalization* but not to *adversarial training for robustness*. As a result, the GIF encourages the model to predict invariantly in the cluster of each class. Experiments demonstrate that the GIF can indeed enhance adversarial robustness on various adversarial training methods and various datasets.

1 Introduction

Deep neural networks (DNNs) trained with a standard learning procedure are vulnerable to *adversarial data* (Biggio et al., 2013; Szegedy et al., 2014; Goodfellow et al., 2015; Nguyen et al., 2015). *Adversarial training* (AT) is one of the most effective strategies for enhancing the model robustness against the adversarial data (Madry et al., 2018). To obtain the *adversarial robustness*, AT methods alternatively generate adversarial data and optimize model parameters on the generated adversarial data (Madry et al., 2018; Cai et al., 2018; Wang et al., 2019; 2020; 2021; Zhang et al., 2019; 2020; Pang et al., 2019a; 2020; 2021; Wu et al., 2020; B.S. and Babu, 2020; Wong et al., 2020; Rice et al., 2020; Sriramanan et al., 2020; Bai et al., 2021).

Recent studies on AT suggest the unequal treatment of data (Ding et al., 2020; Wang et al., 2019; 2020; Zhang et al., 2021a). In particular, Zhang et al. (2021a) divided the training data into two categories—*attackable data* and *guarded data*, in which attackable/guarded data are close to/far away from the class boundary that can/cannot be attacked. To enhance adversarial robustness, attackable data are particularly useful in learning the decision boundary (Wang et al., 2020; Zhang et al., 2021a).

However, as the AT progresses, the ratio of attackable data decreases significantly, which jeopardizes the enhancement of adversarial robustness. In Figure 1, we plot the ratio of attackable data in the left panel and the robust accuracy in the right panel. The red lines show the training dynamics of a typical AT method (Madry et al., 2018). As the training progresses, more and more training data become guarded; thus, the ratio of attackable data decreases. After Epoch 30 (with a reduced learning rate), this ratio drops rapidly, while the robust accuracy ceases to rise but begins to drop. This strong correlation between this ratio and the robustness urges us to introduce more attackable data for AT.

A straightforward remedy for the shortage of attackable data is to incorporate more training data (Schmidt et al., 2018). Schmidt et al. (2018) and Hendrycks et al. (2019) showed that AT for learning a robust model requires substantially more training data than *standard training* (ST). Nevertheless, gathering additional data especially with high-quality

*Equal contributions.

†Corresponding author.

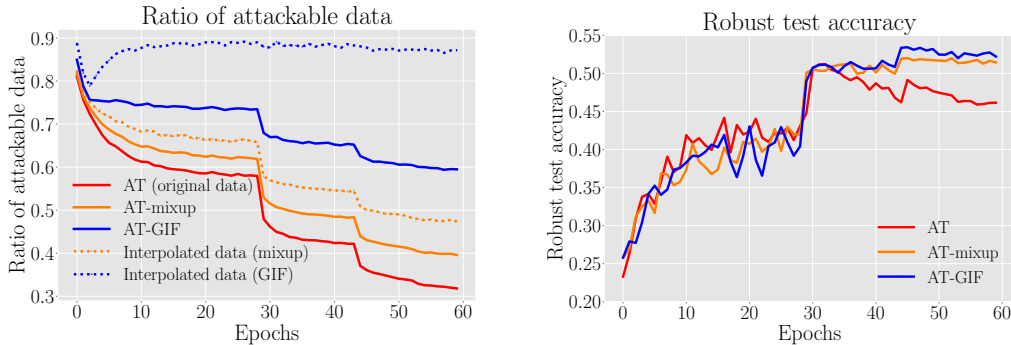


Figure 1: Comparisons between AT (Madry et al., 2018), AT-mixup (AT with vanilla mixup), and AT-GIF (AT with our GIF) on the CIFAR-10 dataset (Krizhevsky et al., 2009). The detailed experimental settings are in Appendix B.1. **Left panel:** The attackable data ratio of AT (red line) decreases rapidly as the training progresses. In each mini-batch, both AT-mixup and AT-GIF use 50% original data and 50% interpolated data for adversarial training. Among the interpolated data (dotted lines), nearly 90% by the GIF (blue dotted line) are attackable, while the interpolated data by vanilla mixup (orange dotted line) contain a much lower ratio of attackable data. Therefore, compared with AT-mixup (orange solid line), AT-GIF (blue solid line) can leverage a higher ratio of attackable data per epoch. **Right panel:** The robust test accuracy is evaluated under PGD-20 attack. The robust test accuracy of AT (red line) rises when the attackable data ratio is high (before Epoch 30). After Epoch 30 (with a reduced learning rate), the robust test accuracy drops significantly, which is strongly related to the low ratio of attackable data. Compared with AT-mixup (orange solid line), AT-GIF (blue solid line) has a higher robust accuracy.

labels is often expensive; therefore, Carmon et al. (2019), Alayrac et al. (2019), and Najafi et al. (2019) leveraged a massive amount of unlabeled data for training adversarially robust models. However, in many privacy-sensitive applications such as medicine (Buch et al., 2018) and finance (Abbe et al., 2012), collecting massive unlabeled data is very costly and sometimes not possible at all (Voigt and Bussche, 2017).

To mitigate this shortage, this paper proposes a novel data augmentation framework—the *guided interpolation framework* (GIF)—for AT. Without collecting massively additional data, the GIF employs the meta information of the previous epoch to guide the data’s interpolation, and then, the interpolated data are used for the current-epoch training (details in Section 3.2). As shown in Figure 1, compared with vanilla-mixup AT (AT-mixup, orange line), the AT with GIF (AT-GIF, blue line) has a higher ratio of attackable data, leading to a higher robust accuracy.

In particular, the GIF is carefully designed for AT, which mitigates the *model’s linear behavior between classes*. The model’s linear behavior is introduced by the vanilla mixup (Zhang et al., 2018); it encourages the model predictions that transit linearly from class to class, providing a smooth change of prediction confidence (Zhang et al., 2018) (two middle panels of Figure 2). However, this linear behavior is favorable to ST for the generalization (and weak robustness against FGSM attack (Zhang et al., 2021b)) but not to AT for the strong robustness against the adaptive attacks. AT encourages the model to be locally constant within the input’s neighborhood (Papernot et al., 2016; Goodfellow et al., 2015), thus encouraging invariant predictions within the cluster of each class (two left panels of Figure 2). To this end, the GIF mitigates defect of vanilla mixup (i.e., introducing the linear behavior) and encourages invariant predictions (two right panels of Figure 2); it meanwhile can generate more attackable data, thus further enhancing the robustness.

We summarize our contributions as follows.

- Although the vanilla mixup (Zhang et al., 2018) can indeed generate more attackable data (compared with AT), we show that it meanwhile introduces the model’s linear behavior between classes, which is never our desideratum for adversarial robustness (Section 3.1).
- We design a novel guided interpolation framework (GIF) for adversarial training (AT). To enhance adversarial robustness, the GIF can mitigate the undesirable linear behaviors and meanwhile provide more attackable data (Section 3). Moreover, the GIF is a compatible approach: it can be easily incorporated into existing adversarial training methods, e.g., TRADES (Zhang et al., 2019) and GAIRAT (Zhang et al., 2021a).
- Experiments on various datasets and adversarial training methods corroborate the efficacy of our GIF in enhancing adversarial robustness (Section 4).

2 Preliminary and Related Work

Section 2.1 reviews a typical AT method, i.e., standard adversarial training by Madry et al. (2018), and reviews recent other AT methods that claimed the unequal treatment of data. Section 2.2 reviews the mixup (Zhang et al., 2018) and its relation with robustness. We also highlight the difference between our GIF and existing studies.

2.1 Adversarial Training

Let (x, d_∞) be the input feature space \mathcal{X} with the infinity distance metric $d_\infty(x, x') = \|x - x'\|_\infty$, and $\mathcal{B}_\epsilon(x) = \{x' \in \mathcal{X} | d_\infty(x, x') < \epsilon\}$ be the closed ball of radius $\epsilon > 0$ centered at x in \mathcal{X} . Let $S = \{(x_i, y_i)\}_{i=1}^n$ be a dataset, where $x_i \in \mathcal{X}$ is the input, and $y_i \in \mathcal{Y}$ is the one-hot label of x_i . Let C be the number of classes, $f^c(\cdot)$ be the c -th element of the model’s prediction $f(\cdot)$, and y^c be the c -th element of one-hot label y .

2.1.1 Standard Adversarial training

The objective function of standard adversarial training (AT) (Madry et al., 2018) is

$$\min_{f_\theta \in \mathcal{F}} \frac{1}{n} \sum_{i=1}^n \ell(f_\theta(\tilde{x}_i), y_i), \quad (1)$$

where

$$\tilde{x}_i = \arg \max_{\tilde{x} \in \mathcal{B}_\epsilon(x_i)} \ell(f_\theta(\tilde{x}), y_i). \quad (2)$$

\tilde{x}_i is the most adversarial data within the ϵ -ball centered at x . $f_\theta(\cdot) : \mathcal{X} \rightarrow \mathbb{R}^C$ is a score function with parameters θ . $\ell : \mathbb{R}^C \times \mathcal{Y} \rightarrow \mathbb{R}$ is the loss function (e.g., the cross-entropy loss). Adversarial training can be divided into two steps: The first step maximizes the loss to find adversarial data; the second step minimizes the loss on the adversarial data w.r.t. the parameters θ .

Standard AT uses projected gradient descent (PGD) to approximate Eq. (2) and generate adversarial data. Given a starting point $x^{(0)} \in \mathcal{X}$, step size $\alpha > 0$, radius $\epsilon > 0$, and maximum number of steps K , PGD searches adversarial data as follows:

$$x^{(k+1)} = \Pi_{\mathcal{B}_\epsilon(x^{(0)})} \left(x^{(k)} + \alpha \text{sign}(\nabla_{x^{(k)}} \ell(f_\theta(x^{(k)}), y)) \right), \quad (3)$$

where $k = 0, \dots, K - 1$ is the step number, $x^{(0)}$ refers to natural data or natural data perturbed by a small Gaussian or uniform random noise, y is the corresponding label for the natural data, $x^{(k)}$ is the adversarial data at step k , and $\Pi_{\mathcal{B}_\epsilon(x^{(0)})}(\cdot)$ projects the adversarial data onto the ϵ -ball centered at x^0 . Eq. (3) increases the loss by gradient ascent and then projects the updated adversarial data back onto the ϵ -ball centered at x^0 .

After K steps of PGD, standard AT utilizes the generated adversarial data x^K to update the model parameters θ . On evaluation, the *robust accuracy* is used, which is the fraction of predictions that the model correctly makes on the adversarial data generated by the adversarial attacks such as the PGD attack (in Eq. (3)).

2.1.2 Unequal treatment of data in AT

Recent studies (Ding et al., 2020; Wang et al., 2020; Cheng et al., 2020; Zhang et al., 2021a) showed that data do not contribute equally during adversarial training. Max-margin adversarial training (MMA) (Ding et al., 2020) demonstrated that adversarial data close to the model’s decision boundary are more important to the robust model, while adversarial data far from the decision boundary are less important. Misclassification aware adversarial training (MART) (Wang et al., 2020) differentiated the misclassified and correctly classified data during AT. Customized adversarial training (CAT) (Cheng et al., 2020) adaptively customized the perturbation bound and the corresponding label for each training data according to their distance to the decision boundary. Geometry-aware instance-reweighted adversarial training (GAIRAT) (Zhang et al., 2021a) paid more attention to data close to the decision boundary. Specifically, GAIRAT split all the data into two categories—*attackable data* and *guarded data*. Data close to the decision boundary are called attackable data, while guarded data are far from the decision boundary. Formally, a sample (x, y) is said to be attackable, if

$$\arg \max_c f_\theta^c(\tilde{x}) \neq \arg \max_c y^c, \quad (4)$$

where \tilde{x} is the adversarial variant of natural data x . On the other hand, a sample (x, y) is said to be guarded, if

$$\arg \max_c f_\theta^c(\tilde{x}) = \arg \max_c y^c. \quad (5)$$

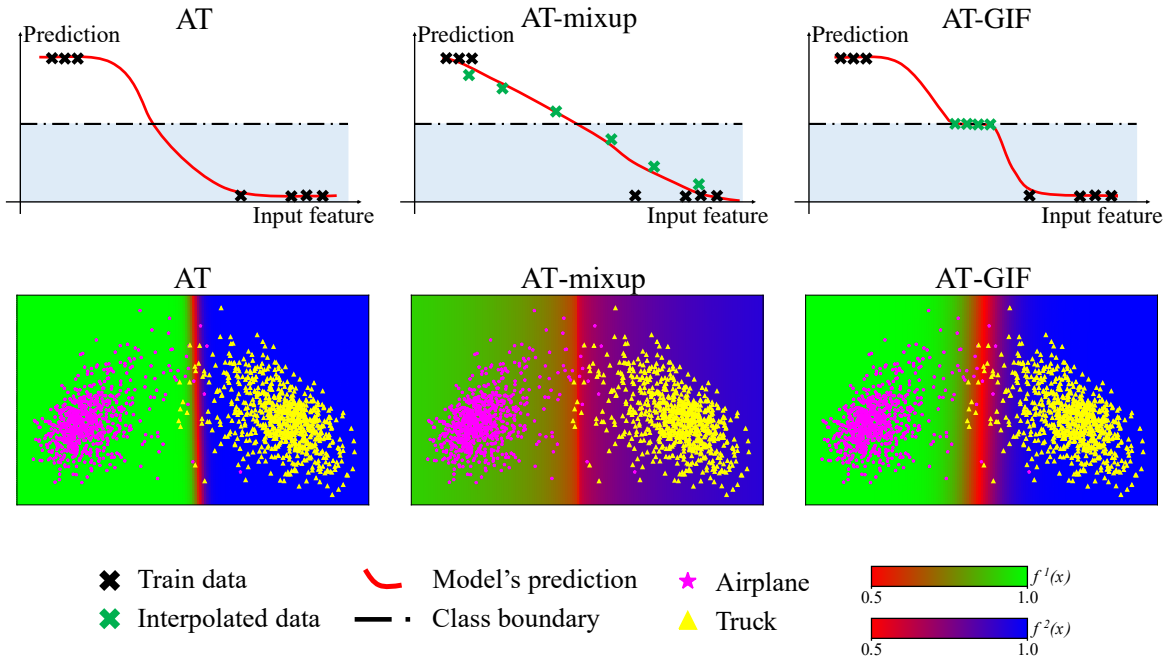


Figure 2: Comparisons between AT, AT-mixup, and AT-GIF. **The three upper panels** illustrate AT, AT-mixup, and AT-GIF, respectively. The horizontal axis is the input feature, and the vertical axis is the prediction of data. The data in blue shade are predicted as the first label, and the data outside the blue shade are predicted as the second label. **The three lower panels** show the experimental results of AT, AT-mixup, and AT-GIF, respectively. The data are randomly selected from the CIFAR-10 dataset. The detailed settings are in Appendix B.1. Red-green shading represents $f^1(x)$ (the prediction confidence for “airplane”), and red-blue shading represents $f^2(x)$ (the prediction confidence for “truck”). **The two left panels** indicate that the standard AT has a sharp transition between the two classes. **The two middle panels** demonstrate that AT-mixup leads to the model’s linear behavior between classes: the prediction confidence changes smoothly. **The two right panels** suggest that AT-GIF can obtain more attackable data by interpolation (see Figure 1) and still keeps a sharper transition between the two classes: the prediction confidence changes abruptly. Besides, in Appendix C.1, we conduct an auxiliary experiment to further compare the differences between AT, AT-mixup, and AT-GIF on ResNet-18 (He et al., 2016). We visualize the linear behavior of AT-mixup, and show that AT-GIF can alleviate the linear behavior.

The adversarial variants of attackable data can be easily misclassified, while guarded data’s adversarial variants are hard to be misclassified. GAIRAT claimed that attackable data help to improve adversarial training, while the guarded data are less important.

We propose a guided interpolation framework (GIF), which utilizes the meta information of the previous epoch to guide the data’s interpolation. The GIF can obtain a high ratio of attackable data to enhance AT. Compared to the widely used vanilla mixup (Zhang et al., 2018), the GIF can obtain more attackable data by interpolation and mitigate the linear behavior of the vanilla mixup (see Figure 1, 2 and Section 3.2 for details), which is beneficial to AT. Furthermore, the GIF can be incorporated into existing AT methods (e.g., AT (Madry et al., 2018), TRADES (Zhang et al., 2019), GAIRAT (Zhang et al., 2021a), and FastAT (Wong et al., 2020)) and improve their robustness (see Section 4.1 for details).

2.2 Mixup for Robustness

In standard training (ST), mixup has been widely used to improve the generalization (Zhang et al., 2018; Thulasidasan et al., 2019; Berthelot et al., 2019; 2020; Kim et al., 2021; Zhang et al., 2021b). Mixup augments the original dataset with interpolated data as follows.

$$\begin{aligned}\bar{x} &= \lambda x_i + (1 - \lambda)x_j, \\ \bar{y} &= \lambda y_i + (1 - \lambda)y_j,\end{aligned}\tag{6}$$

Algorithm 1 Adversarial training with guided interpolation framework (AT-GIF)

Input: model f_θ , training dataset S , learning rate η , number of epochs T , original batch size m , interpolation batch size m' , number of batches M , perturbation bound ϵ , step size α , PGD step number K

Output: adversarially robust network f_θ

```
 $A_0 \leftarrow S$ 
for epoch  $t = 1, 2, \dots, T$  do
   $A_t = \emptyset$ 
  Compute interpolation set  $\bar{S}_t$  by  $A_{t-1}$  and Eq. (9)
  for mini-batch  $= 1, \dots, M$  do
    Randomly sample  $\{(x_i, y_i)\}_{i=1}^m$  from  $S$ 
    for  $i = 1, \dots, m$  do in parallel
      Generate adversarial data  $\tilde{x}_i$  of  $x_i$  by Eq. (3)
      if  $\arg \max_c f_\theta^c(\tilde{x}_i) \neq \arg \max_c y_i^c$  then
         $A_t \leftarrow A_t \cup \{(x_i, y_i)\}$ 
      end if
    end for
    Randomly sample  $\{(x_i, y_i)\}_{i=m+1}^{m+m'}$  from  $\bar{S}_t$ 
    for  $i = m + 1, \dots, m + m'$  do in parallel
      Generate adversarial data  $\tilde{x}_i$  of  $x_i$  by Eq. (3)
    end for
     $\theta \leftarrow \theta - \eta \cdot \frac{1}{m+m'} \sum_{i=1}^{m+m'} \nabla_{\theta} \ell(f_\theta(\tilde{x}_i), y_i)$ 
  end for
end for
```

where (\bar{x}, \bar{y}) is the interpolated data, (x_i, y_i) and (x_j, y_j) are two randomly selected data from the original dataset S , and λ is the interpolation weight. Zhang et al. (2021b) showed that mixup (in ST) can improve the robustness against fast gradient sign attack (FGSM) (Goodfellow et al., 2015). Nevertheless, mixup (in ST) fails to defend stronger adaptive attacks (e.g., PGD (Madry et al., 2018) and CW attack (Carlini and Wagner, 2017)) (Zhang et al., 2018).

To defend against adaptive attacks, several mixup-based adversarial training techniques have been proposed (Lamb et al., 2019; Laugros et al., 2020). Interpolated adversarial training (IAT) (Lamb et al., 2019) trains on interpolations of adversarial data along with interpolations of natural data. Mixup with targeted labeling adversarial training (M-TLAT) (Laugros et al., 2020) combines vanilla mixup with targeted labeling to enhance AT. However, these methods behave linearly when employing vanilla mixup in AT, and such linear behaviors will damage the adversarial robustness (see Section 3.1 for details). To alleviate this issue, we propose the GIF for AT, which aims to obtain a high ratio of attackable data by interpolation and mitigate the linear behavior (see Section 3.2 for details).

Pang et al. (2019b) proposed mixup inference (MI) to exploit the linear behaviors of the mixup-based models in the inference phase, while our work concentrates on investigating data interpolation in the training phase.

3 Guided Interpolation Framework (GIF)

In this section, we present our motivation and introduce our proposed guided interpolation framework (GIF).

3.1 Motivation of GIF

Enhancing adversarial robustness further requires abundant attackable data. As discussed in Section 2.1.2, data contribute unequally during AT, and more attackable data can better benefit the robustness enhancement. The left panel of Figure 1 indicates both vanilla mixup (orange dotted line) (Zhang et al., 2018) and the GIF (blue dotted line) can introduce a higher ratio of attackable data (compared to standard AT). The right panel of Figure 1 shows AT-mixup and AT-GIF can indeed improve adversarial robustness. This suggests that utilizing mixup or GIF is helpful to AT.

Adversarial robustness requires the local invariance. Goodfellow et al. (2015), Papernot et al. (2016), and Zhang et al. (2021a) demonstrated that in AT, the model predictions are supposed to be locally invariant to the inputs' neighborhood. Ding et al. (2020) proposed to maximize the distances from the inputs to the model's decision boundary, which encouraged the invariant predictions in the inputs' neighbourhood. The above studies all show that a well-trained adversarial model should be locally invariant. This infers the model's linear behavior is never AT's desideratum.

However, directly employing vanilla mixup in AT will lead to the linear behavior. Figure 2 shows that the prediction of AT-mixup (two middle panels) moves linearly from one class to the other, while standard AT (two left panels) has a sharp transition between the two classes. Although AT-mixup can introduce more attackable data to improve adversarial robustness, it inevitably involves undesirable linear behavior in AT.

The above observation motivates us to obtain more attackable data by interpolation meanwhile without sacrificing much the local invariance.

3.2 Realization of GIF

In mixup, each interpolated data is computed by two different data (Eq. (6)), which results in a soft interpolated label $\bar{y} \in [0, 1]^C$. Let (\bar{x}, \bar{y}) be an interpolated data computed by (x_i, y_i) and (x_j, y_j) (with Eq. (6)), \tilde{x} be the adversarial variant of \bar{x} computed with Eq. (3). We say the interpolated data (\bar{x}, \bar{y}) is attackable, if

$$\arg \max_c f_\theta^c(\tilde{x}) \neq \arg \max_c y_i^c \wedge \arg \max_c f_\theta^c(\tilde{x}) \neq \arg \max_c y_j^c, \quad (7)$$

where \wedge is "And" operation. Otherwise, we say it is guarded, if

$$\arg \max_c f_\theta^c(\tilde{x}) = \arg \max_c y_i^c \vee \arg \max_c f_\theta^c(\tilde{x}) = \arg \max_c y_j^c, \quad (8)$$

where \vee is "Or" operation.

According to Eq. (6), there are two core factors in data interpolation: 1) selecting data for interpolation and 2) setting the interpolation weight λ .

The first part is selecting data for interpolation. Vanilla mixup randomly picks data for interpolation. The attackable ratio of interpolated data also drops rapidly as adversarial training progresses (see the orange dotted line in the left panel of Figure 1). To alleviate this issue, our GIF only chooses attackable data (see Eq.(4)) for interpolation; thus, the interpolated data are more likely to be attackable (see the blue dotted line in the left panel of Figure 1).

The second part is setting the interpolation weight λ . In vanilla mixup, λ is sampled randomly from a uniform (or beta) distribution, which is not suitable in adversarial training. A uniformly sampled λ will encourage the model to behave linearly between classes, which is not in favor of AT. The two middle panels of Figure 2 show that AT-mixup has a linear transition, which is not favorable to AT. Instead of random sampling from a uniform distribution, we argue to fix $\lambda = 0.5$. By fixing $\lambda = 0.5$, we can mitigate the linear behavior between classes (see AT-GIF in Figure 2). Thus, fixing $\lambda = 0.5$ will benefit AT. We also discuss the effect of different interpolation weight λ in Section 4.2.

In summary, we interpolate data as follows:

$$\begin{aligned} \bar{x} &= 0.5x_i + 0.5x_j \\ \bar{y} &= 0.5y_i + 0.5y_j, \end{aligned} \quad (9)$$

where (\bar{x}, \bar{y}) is the interpolated data, (x_i, y_i) and (x_j, y_j) are two random attackable data satisfying Eq. (4). In the left panel of Figure 1, the attackable ratio of data interpolated by the GIF (blue dotted line) is stabled at around 90%, which indicates our interpolation strategy can indeed increase the ratio of attackable data. Besides, the two right panels of Figure 2 also demonstrate that AT-GIF (with $\lambda = 0.5$) behaves sharply between classes. Therefore, our GIF is beneficial to the enhancement of the adversarial robustness.

The training of AT-GIF is shown in Algorithm 1. First, at the beginning of each epoch, we obtain the interpolation set from the previous attackable set (computed in the previous epoch). Second, we generate the adversarial variants of data from the original dataset along with the interpolation set for updating the model. Third, we filter out the attackable data from the original dataset and put them into the current attackable set A . This attackable set A will be used to obtain the interpolation set that guides the next-epoch training. Last, we compute the loss of the adversarial variants and update the parameters θ with the gradient of the loss.

In Algorithm 1, a burn-in period may be introduced. During the initial period of the training epochs, instead of generating data with the GIF, we utilize the original data without the need for the interpolated data for the AT. This is because, during the initial period, standard AT has a high ratio of attackable data which is enough for the enhancement of the adversarial robustness. We also discuss the effect of the burn-in period in Section 4.2.

Figure 1 and 2 show the differences between standard AT, AT-mixup (AT with vanilla mixup), and AT-GIF (AT with GIF). The left panel of Figure 1 demonstrates that the GIF can obtain nearly 90% of attackable data by interpolation (blue dotted line), which is much higher than the interpolated data by vanilla mixup (orange dotted line) and the original data (red line). The right panel of Figure 1 manifests that our AT-GIF can indeed improve robustness with a higher ratio

Table 1: Test accuracy of ResNet-18 on the CIFAR-10 dataset.

Defense	Best				Last			
	Natural	PGD-20	CW	AA	Natural	PGD-20	CW	AA
AT (Madry et al., 2018)	81.72	51.05	49.86	47.25	84.77	45.47	45.90	43.28
IAT (Lamb et al., 2019)	90.61	41.11	41.93	36.43	90.53	39.50	40.43	35.10
$KD_{std&adv} + SWA$ (Chen et al., 2021)	85.16	46.85	46.73	44.74	85.63	45.45	46.12	43.70
AT-GIF (Ours)	81.59	53.57	50.07	47.91	83.15	52.06	48.21	45.59

Table 2: Test accuracy of WRN-32-10 on the CIFAR-10 dataset.

Defense	Best				Last			
	Natural	PGD-20	CW	AA	Natural	PGD-20	CW	AA
AT (Madry et al., 2018)	86.73	53.66	53.66	50.96	86.88	47.94	48.12	45.82
IAT (Lamb et al., 2019)	95.79	50.85	49.53	11.51	96.55	47.37	48.50	3.87
$KD_{std&adv} + SWA$ (Chen et al., 2021)	84.46	52.73	52.53	50.85	86.53	50.34	50.29	48.07
AT-GIF (Ours)	86.49	55.92	53.99	51.92	86.14	51.42	49.17	46.70

of attackable data. Figure 2 indicates that AT-mixup (two middle panels) leads to the robust model that behaves linearly, while the robust models trained by AT (two left panels) and AT-GIF (two right panels) have a sharper transition between different classes; inside each class, the model’s predictions are almost invariant. Therefore, AT-GIF can obtain more attackable data by the interpolation and meanwhile keep the local invariance. As a result, AT-GIF can lead to a more robust model against the adversarial attacks.

4 Experiments

In this section, we empirically justify the efficacy of our proposed GIF on CIFAR-10 (Krizhevsky et al., 2009) and SVHN (Netzer et al., 2011) datasets. The detailed descriptions of the two datasets are in Appendix B.2. All models are trained with ResNet-18 (He et al., 2016) or Wide ResNet (WRN) (Zagoruyko and Komodakis, 2016). All experiments are run on the same machine with Intel Xeon Gold 5218 CPU, 250GB RAM, and six NVIDIA Tesla V100 SXM2 GPU. All methods are implemented with PyTorch 1.7.0 (Paszke et al., 2019).

Setup. We first introduce the settings for the CIFAR-10 dataset. In our experiments, we consider $\|\tilde{x} - x\|_\infty < \epsilon$ with the same ϵ in both training and evaluations. All images of CIFAR-10 are normalized into $[0, 1]$. We set the original batch size $m = 64$; the interpolation batch size $m' = 64$. For generating the most adversarial data to update the model, the perturbation bound $\epsilon = 8/255$; PGD step number $K = 10$; and PGD step size $\alpha = 2/255$, which keeps the same as (Rice et al., 2020). We train the model using SGD with 0.9 momentum for 60 epochs with the initial learning rate of 0.1 divided by 10 at Epoch 30 and 45, respectively. The weight decay is $5e - 4$. For evaluations, we report standard test accuracy for natural test data and robust test accuracy for adversarial test data. The adversarial test data are generated by PGD-20 attack (PGD attack with 20 steps) (Madry et al., 2018), CW attack (with 30 steps) (Carlini and Wagner, 2017), and Auto attack (AA) (Croce and Hein, 2020) with the same perturbation bound $\epsilon = 8/255$. The step size α for PGD-20 attack and CW attack is $2/255$.

In SVHN, we set the perturbation bound $\epsilon = 4/255$, PGD step size $\alpha = 1/255$, and initial learning rate $\eta = 0.01$. For evaluations, the adversarial test data are generated by PGD-20 attack, CW attack, and Auto attack (AA) with the same perturbation bound $\epsilon = 4/255$. The step size α for PGD-20 attack and CW attack is $1/255$. Other settings of SVHN are the same as CIFAR-10.

We compare our AT-GIF with the following methods: standard adversarial training (AT) (Madry et al., 2018), IAT (Lamb et al., 2019), $KD_{std&adv} + SWA$ (Chen et al., 2021). We also modify TRADES (Zhang et al., 2019), GAIAT (Zhang et al., 2021a), and FastAT (Wong et al., 2020) to their GIF versions, i.e., TRADES-GIF, GAIAT-GIF, and FastAT-GIF, and compare the performance of these methods. The algorithm of TRADES-GIF, GAIAT-GIF, and FastAT-GIF are shown in Appendix A.

For fair comparisons, instead of sampling interpolated data from the interpolation set \bar{S} in GIF-based methods, all baseline methods set the original batch size $m = 128$ and the interpolation batch size $m' = 0$, i.e., we make sure that all methods train on the same amount of data. All GIF-based methods (e.g., AT-GIF, TRADES-GIF, GAIAT-GIF, and FastAT-GIF) involve a burn-in period except the models trained in Figure 1 and Figure 2. The detailed settings of all these methods are in Appendix B.3.

Table 3: Test accuracy of GIF incorporating with other AT methods on the CIFAR-10 dataset.

Defense	Network	Best				Last			
		Natural	PGD-20	CW	AA	Natural	PGD-20	CW	AA
TRADES	WRN-34-10	84.92	55.33	53.81	52.54	85.10	53.16	51.12	50.09
TRADES-GIF		83.64	57.45	54.14	53.37	84.25	56.91	53.91	53.08
GAIRAT	WRN-32-10	86.31	56.69	44.63	42.26	85.43	52.50	43.71	41.14
GAIRAT-GIF		84.59	64.97	46.71	44.84	82.18	55.11	45.65	43.24
FastAT	WRN-32-10	88.38	46.14	47.31	43.70	89.56	6.79	6.01	0.03
FastAT-GIF		88.83	48.42	48.26	41.91	89.93	0.39	0.34	0.00

4.1 Robustness Evaluation

In this section, we first evaluate the robustness of AT-GIF on the CIFAR-10 dataset. Then, we show that the GIF can be easily incorporated into modern adversarial training methods (e.g., TRADES, GAIRAT, and FastAT). Last, we demonstrate that the GIF can also improve robustness on the SVHN dataset.

Robustness evaluation on CIFAR-10. We first show the efficiency of the GIF on CIFAR-10. We compare AT-GIF with standard AT, IAT, and $KD_{std&adv} + SWA$.

In Table 1, we report the test accuracy of these models trained with ResNet-18. To keep the same setting as (Madry et al., 2018), we also report the performance of WRN-32-10 in Table 2. AT-GIF achieves the best adversarial robustness. For example, AT-GIF improves the best robust accuracy of AT by 2.52% on ResNet-18 under PGD-20 attack. The results indicate that AT suffers from overfitting, and has a large robust accuracy drop in the last epoch. AT-GIF alleviates the overfitting issue by interpolating more attackable data. The results also demonstrate that AT-GIF outperforms vanilla mixup-based methods (e.g., IAT), which further verifies the design of the GIF is more suitable (than vanilla mixup) in AT. $KD_{std&adv} + SWA$ mitigates the overfitting problem, but can hardly improve the robustness. AT-GIF can alleviate the overfitting issue and improve robustness at the same time.

Robustness evaluation of GIF incorporating with other AT methods. To show the GIF is a compatible approach, we compare TRADES, GAIRAT, and FastAT with their GIF versions, i.e., TRADES-GIF, GAIRAT-GIF, and FastAT-GIF.

Table 3 demonstrates the results of these methods trained with Wide ResNet on the CIFAR-10 dataset. To make fair comparisons, TRADES and TRADES-GIF are trained with WRN-34-10 (Zhang et al., 2019), and other methods are trained with WRN-32-10 (Zhang et al., 2021a; Wong et al., 2020). We also report the results of these models trained with ResNet-18 on the CIFAR-10 dataset in Appendix C.2. The GIF versions (TRADES-GIF, GAIRAT-GIF, and FastAT-GIF) have a better performance than their original versions (TRADES, GAIRAT, and FastAT). For instance, GAIRAT-GIF increases the robust test accuracy of GAIRAT by 8.28% on WRN-32-10 under PGD-20 attack. The failure of FastAT and FastAT-GIF in the last epoch is due to catastrophic overfitting (Wong et al., 2020).

Robustness evaluation on SVHN. We report the performance of AT-GIF compared with AT on the SVHN dataset in Table 4. AT-GIF can improve the test accuracy of AT by 3.46% on ResNet-18 under PGD-20 attack. This manifests that the GIF can indeed improve adversarial robustness on various datasets.

4.2 Ablation Studies

In this section, we conduct a series of ablation studies to further understand the effects of different components in AT-GIF.

Generating adversarial training data with CW attack. Besides PGD-10 attack, we also utilize the CW attack (Carlini and Wagner, 2017) with 10 steps (CW-10) to generate adversarial training data (Eq. (3)) on ResNet-18. Table 5 reports the results of generating adversarial training data with PGD-10 (AT-GIF (PGD)) and CW-10 (AT-GIF (CW)). AT-GIF (CW) increases the robust test accuracy by 6.08% on PGD-20 attack but has a lower performance on CW attack. The results show that generating adversarial training data with CW attack is also promising.

Selection of the interpolation weight λ . We report the robustness of our fixed $\lambda = 0.5$ with a random λ sampled from a uniform distribution or a beta distribution, i.e., $\lambda \sim \mathcal{U}(0, 1)$ or $\lambda \sim \text{Beta}(0.3, 0.3)$ in Figure 3. The hyperparameters for uniform distribution and beta distribution are set according to (Zhang et al., 2018). When $\lambda = 0.5$ (blue line), the

Table 4: Test accuracy of ResNet-18 on the SVHN dataset.

Defense	Natural	PGD-20	CW
AT	95.67	74.52	74.86
AT-GIF	94.98	77.98	75.10

Table 5: Test accuracy of AT-GIF with different methods of generating adversarial training data on the CIFAR-10 dataset.

Defense	Natural	PGD-20	CW
AT-GIF (PGD)	81.59	53.57	50.07
AT-GIF (CW)	81.19	59.65	47.79

model achieves the best performance, which shows that $\lambda = 0.5$ can indeed improve robustness. The model with $\lambda \sim \mathcal{U}(0, 1)$ (orange line) underperforms our AT-GIF with a fixed $\lambda = 0.5$, due to that the uniform distribution of λ leads to undesirable linear behavior.

In addition, we report the robustness of AT-GIF with different fixed interpolation weight $\lambda \in \{0.1, 0.2, \dots, 0.5\}$ on the CIFAR-10 dataset in Appendix C.3. The results show that fixing $\lambda = 0.5$ achieves the best robustness, which further verifies the GIF indeed aids in AT.

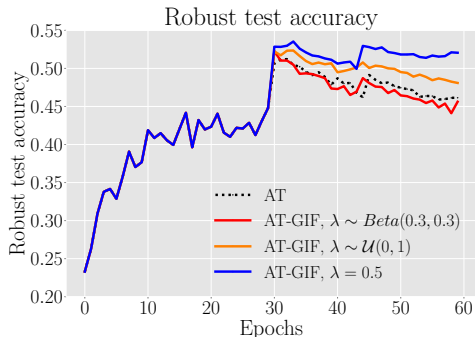


Figure 3: Robust test accuracy of AT-GIF with different λ under PGD-20 attack.

The effects of the burn-in period. We conduct an experiment to show the effects of the burn-in period on ResNet-18. Table 6 compares the performance of AT-GIF with and without the burn-in period. AT-GIF (burn-in) trains with the original data without the need of the interpolated data in the first 30 epochs, and start to train with both the original data and the interpolated data after Epoch 30. AT-GIF (naive) utilizes the original data and the interpolated data for adversarial training from the first epoch. The results suggest that the burn-in period can slightly improve the robustness under CW attack, but has a slightly lower test accuracy under PGD-20 attack.

Table 6: Test accuracy of AT-GIF with and without the burn-in period on the CIFAR-10 dataset.

Defense	Natural	PGD-20	CW
AT-GIF (naive)	82.35	53.60	49.13
AT-GIF (burn-in)	81.59	53.57	50.07

Different ratios of original data and interpolated data. We train AT-GIF with different ratios of data from the original dataset and the interpolation set (e.g., 1:1, 1:2, and 2:1). To make sure these methods train with the same amount of data in one mini-batch, in AT-GIF (1:1), we set original batch size $m = 64$ and interpolation batch size $m' = 64$; in AT-GIF (1:2), we set $m = 43$ and $m' = 85$; and in AT-GIF (2:1), we set $m = 85$ and $m' = 43$. We report the test accuracy of these models in Appendix C.4. AT-GIF (1:1) has a better performance than AT-GIF (1:2) and AT-GIF (2:1). This indicates that selecting an appropriate ratio of the original data and the attackable data is also important for robustness enhancement.

5 Conclusion

This paper has proposed a novel data augmentation framework, i.e., guided interpolation framework (GIF), for adversarial training. The GIF utilizes the meta information of the previous epoch to guide the data interpolation process. GIF can obtain a high ratio of attackable data by interpolation without sacrificing much the local invariance, efficiently enhancing adversarial robustness. Extensive experiments show our GIF boosts the robustness of AT. A promising future direction is to investigate the different impacts of attackable data and guarded data in AT.

6 Acknowledgement

This work was supported by the Key Research and Development Program of Zhejiang Province of China (No. 2020C01024), and the National Natural Science Foundation of China under Grant No. 62050099, and the Natural Science Foundation of Zhejiang Province of China (No. LY18F020005). JZ, GN, and MS were supported by JST AIP Acceleration Research Grant Number JPMJCR20U3, Japan. MS was also supported by the Institute for AI and Beyond, UTokyo.

References

- Battista Biggio, Igino Corona, Davide Maiorca, Blaine Nelson, Nedim Šrđić, Pavel Laskov, Giorgio Giacinto, and Fabio Roli. Evasion attacks against machine learning at test time. In *Joint European conference on machine learning and knowledge discovery in databases*, pages 387–402. Springer, 2013.
- Christian Szegedy, Wojciech Zaremba, Ilya Sutskever, Joan Bruna, Dumitru Erhan, Ian Goodfellow, and Rob Fergus. Intriguing properties of neural networks. In *ICLR*, 2014.
- Ian J Goodfellow, Jonathon Shlens, and Christian Szegedy. Explaining and harnessing adversarial examples. In *ICLR*, 2015.
- Anh Nguyen, Jason Yosinski, and Jeff Clune. Deep neural networks are easily fooled: High confidence predictions for unrecognizable images. In *CVPR*, pages 427–436, 2015.
- Aleksander Madry, Aleksandar Makelov, Ludwig Schmidt, Dimitris Tsipras, and Adrian Vladu. Towards deep learning models resistant to adversarial attacks. In *ICLR*, 2018.
- Qi-Zhi Cai, Chang Liu, and Dawn Song. Curriculum adversarial training. In *IJCAI*, 2018.
- Yisen Wang, Xingjun Ma, James Bailey, Jinfeng Yi, Bowen Zhou, and Quanquan Gu. On the convergence and robustness of adversarial training. In *ICML*, 2019.
- Yisen Wang, Difan Zou, Jinfeng Yi, James Bailey, Xingjun Ma, and Quanquan Gu. Improving adversarial robustness requires revisiting misclassified examples. In *ICLR*, 2020.
- Ren Wang, Kaidi Xu, Sijia Liu, Pin-Yu Chen, Tsui-Wei Weng, Chuang Gan, and Meng Wang. On fast adversarial robustness adaptation in model-agnostic meta-learning. In *ICLR*, 2021.
- Hongyang Zhang, Yaodong Yu, Jiantao Jiao, Eric Xing, Laurent El Ghaoui, and Michael I Jordan. Theoretically principled trade-off between robustness and accuracy. In *ICML*, 2019.
- Jingfeng Zhang, Xilie Xu, Bo Han, Gang Niu, Lizhen Cui, Masashi Sugiyama, and Mohan Kankanhalli. Attacks which do not kill training make adversarial learning stronger. In *ICML*, 2020.
- Tianyu Pang, Kun Xu, Chao Du, Ning Chen, and Jun Zhu. Improving adversarial robustness via promoting ensemble diversity. In *ICML*, 2019a.
- Tianyu Pang, Kun Xu, Yinpeng Dong, Chao Du, Ning Chen, and Jun Zhu. Rethinking softmax cross-entropy loss for adversarial robustness. In *ICLR*, 2020.
- Tianyu Pang, Xiao Yang, Yinpeng Dong, Hang Su, and Jun Zhu. Bag of tricks for adversarial training. In *ICLR*, 2021.
- Dongxian Wu, Shu-Tao Xia, and Yisen Wang. Adversarial weight perturbation helps robust generalization. *NeurIPS*, 33, 2020.
- Vivek B.S. and R. Venkatesh Babu. Single-step adversarial training with dropout scheduling. In *CVPR*, 2020.
- Eric Wong, Leslie Rice, and J. Zico Kolter. Fast is better than free: Revisiting adversarial training. In *ICLR*, 2020.
- Leslie Rice, Eric Wong, and J Zico Kolter. Overfitting in adversarially robust deep learning. In *ICML*, 2020.
- Gaurang Sriramanan, Sravanti Addepalli, Arya Baburaj, and R. Venkatesh Babu. Gama: Guided adversarial margin attack. In *NeurIPS*, 2020.
- Yang Bai, Yuyuan Zeng, Yong Jiang, Shu-Tao Xia, Xingjun Ma, and Yisen Wang. Improving adversarial robustness via channel-wise activation suppressing. In *ICLR*, 2021.
- Gavin Weiguang Ding, Yash Sharma, Kry Yik Chau Lui, and Ruitong Huang. Mma training: Direct input space margin maximization through adversarial training. In *ICLR*, 2020.
- Jingfeng Zhang, Jianing Zhu, Gang Niu, Bo Han, Masashi Sugiyama, and Mohan Kankanhalli. Geometry-aware instance-reweighted adversarial training. In *ICLR*, 2021a.
- Alex Krizhevsky, Geoffrey Hinton, et al. Learning multiple layers of features from tiny images. In *Technical report*, 2009.
- Ludwig Schmidt, Shibani Santurkar, Dimitris Tsipras, Kunal Talwar, and Aleksander Madry. Adversarially robust generalization requires more data. In *NeurIPS*, pages 5014–5026, 2018.
- Dan Hendrycks, Kimin Lee, and Mantas Mazeika. Using pre-training can improve model robustness and uncertainty. In *ICML*, 2019.
- Yair Carmon, Aditi Raghunathan, Ludwig Schmidt, Percy Liang, and John C. Duchi. Unlabeled data improves adversarial robustness. In *NeurIPS*, 2019.

- Jean-Baptiste Alayrac, Jonathan Uesato, Po-Sen Huang, Alhussein Fawzi, Robert Stanforth, and Pushmeet Kohli. Are labels required for improving adversarial robustness? In *NeurIPS*, 2019.
- Amir Najafi, Shin-ichi Maeda, Masanori Koyama, and Takeru Miyato. Robustness to adversarial perturbations in learning from incomplete data. In *NeurIPS*, 2019.
- Varun H Buch, Irfan Ahmed, and Mahiben Maruthappu. Artificial intelligence in medicine: current trends and future possibilities. *Br J Gen Pract.*, 68(668):143–144, 2018.
- Emmanuel A Abbe, Amir E Khandani, and Andrew W Lo. Privacy-preserving methods for sharing financial risk exposures. *American Economic Review*, 102(3):65–70, 2012.
- Paul Voigt and Axel von dem Bussche. *The EU General Data Protection Regulation (GDPR): A Practical Guide*. Springer Publishing Company, Incorporated, 1st edition, 2017. ISBN 3319579584.
- Hongyi Zhang, Moustapha Cisse, Yann N Dauphin, and David Lopez-Paz. mixup: Beyond empirical risk minimization. In *ICLR*, 2018.
- Linjun Zhang, Zhun Deng, Kenji Kawaguchi, Amirata Ghorbani, and James Zou. How does mixup help with robustness and generalization? In *ICLR*, 2021b.
- Nicolas Papernot, Patrick McDaniel, Arunesh Sinha, and Michael Wellman. Towards the science of security and privacy in machine learning. *arXiv:1611.03814*, 2016.
- Kaiming He, Xiangyu Zhang, Shaoqing Ren, and Jian Sun. Deep residual learning for image recognition. In *CVPR*, 2016.
- Minhao Cheng, Qi Lei, Pin-Yu Chen, Inderjit Dhillon, and Cho-Jui Hsieh. Cat: Customized adversarial training for improved robustness. *arXiv:2002.06789*, 2020.
- Sunil Thulasidasan, Gopinath Chennupati, Jeff A Bilmes, Tanmoy Bhattacharya, and Sarah Michalak. On mixup training: Improved calibration and predictive uncertainty for deep neural networks. In *NeurIPS*, pages 13888–13899, 2019.
- David Berthelot, Nicholas Carlini, Ian Goodfellow, Nicolas Papernot, Avital Oliver, and Colin A Raffel. Mixmatch: A holistic approach to semi-supervised learning. In *NeurIPS*, pages 5050–5060, 2019.
- David Berthelot, Nicholas Carlini, Ekin D. Cubuk, Alex Kurakin, Kihyuk Sohn, Han Zhang, and Colin Raffel. Remixmatch: Semi-supervised learning with distribution matching and augmentation anchoring. In *ICLR*, 2020.
- JangHyun Kim, Wonho Choo, Hosan Jeong, and Hyun Oh Song. Co-mixup: Saliency guided joint mixup with supermodular diversity. In *ICLR*, 2021.
- Nicholas Carlini and David A. Wagner. Towards evaluating the robustness of neural networks. In *Symposium on Security and Privacy (SP)*, 2017.
- Alex Lamb, Vikas Verma, Juho Kannala, and Yoshua Bengio. Interpolated adversarial training: Achieving robust neural networks without sacrificing too much accuracy. In *Proceedings of the 12th ACM Workshop on Artificial Intelligence and Security*, pages 95–103, 2019.
- Alfred Laugros, Alice Caplier, and Matthieu Ospici. Addressing neural network robustness with mixup and targeted labeling adversarial training. *arXiv preprint arXiv:2008.08384*, 2020.
- Tianyu Pang, Kun Xu, and Jun Zhu. Mixup inference: Better exploiting mixup to defend adversarial attacks. In *ICLR*, 2019b.
- Tianlong Chen, Zhenyu Zhang, Sijia Liu, Shiyu Chang, and Zhangyang Wang. Robust overfitting may be mitigated by properly learned smoothing. In *ICLR*, 2021.
- Yuval Netzer, Tao Wang, Adam Coates, Alessandro Bissacco, Bo Wu, and Andrew Y Ng. Reading digits in natural images with unsupervised feature learning. In *NeurIPS Workshop on Deep Learning and Unsupervised Feature Learning*, 2011.
- Sergey Zagoruyko and Nikos Komodakis. Wide residual networks. *arXiv:1605.07146*, 2016.
- Adam Paszke, Sam Gross, Francisco Massa, Adam Lerer, James Bradbury, Gregory Chanan, Trevor Killeen, Zeming Lin, Natalia Gimelshein, Luca Antiga, et al. Pytorch: An imperative style, high-performance deep learning library. *NeurIPS*, pages 8026–8037, 2019.
- Francesco Croce and Matthias Hein. Reliable evaluation of adversarial robustness with an ensemble of diverse parameter-free attacks. In *ICML*, 2020.
- Hervé Abdi and Lynne J Williams. Principal component analysis. *Wiley interdisciplinary reviews: computational statistics*, 2(4):433–459, 2010.
- Alex Krizhevsky. Learning multiple layers of features from tiny images. Technical report, 2009.

A Algorithm of TRADES-GIF, GAIRAT-GIF, and FastAT-GIF

To show our GIF is a compatible method, we modify TRADES, GAIRAT, and FastAT to their GIF versions, i.e., TRADES-GIF, GAIRAT-GIF, and Fast-GIF. The training of TRADES-GIF is shown in Algorithm 2. ℓ_{CE} is the cross-entropy loss, ℓ_{KL} is the Killback-Leibler loss, $\mathcal{N}(0, \mathbf{I})$ is the Gaussian distribution with zero mean and identity variance, $\gamma > 0$ is a small constant controlling the strength of the Gaussian distribution, and $\beta > 0$ is the weight of the KL loss. The training of GAIRAT-GIF is shown in Algorithm 3. $\kappa(x, y)$ is the least iteration number that the PGD method need to generate adversarial variant \tilde{x} to fool the network, and $\omega(x, y)$ is the geometry-aware weight assignment function. The training of FastAT-GIF is shown in Algorithm 4. $\mathcal{U}(\cdot, \cdot)$ is the uniform distribution.

Algorithm 2 TRADES with guided interpolation framework (TRADES-GIF)

Input: model f_θ , training dataset S , learning rate η , number of epochs T , original batch size m , interpolation batch size m' , number of batches M , perturbation bound ϵ , step size α , PGD step number K , KL loss weight β , and Gaussian noise weight γ

Output: adversarially robust network f_θ

```

 $A_0 \leftarrow S$ 
for epoch  $t = 1, 2, \dots, T$  do
   $A_t = \emptyset$ 
  Compute interpolation set  $\bar{S}_t$  by  $A_{t-1}$  and Eq. (9)
  for mini-batch  $= 1, \dots, M$  do
    Randomly sample  $\{(x_i, y_i)\}_{i=1}^m$  from  $S$  and  $\{(x_i, y_i)\}_{i=m+1}^{m+m'}$  from  $\bar{S}_t$ 
    for  $i = 1, \dots, m + m'$  do in parallel
       $\tilde{x}_i \leftarrow x_i + \gamma \mathcal{N}(0, \mathbf{I})$ 
      for  $k = 1, \dots, K$  do
         $\tilde{x}_i \leftarrow \Pi_{\mathcal{B}_\epsilon(x_i)}(\alpha \text{sign}(\nabla_{\tilde{x}_i} \ell_{KL}(f_\theta(\tilde{x}_i), f_\theta(x_i))) + \tilde{x}_i)$ 
      end for
      if  $i \leq m$  and  $\arg \max_c f_\theta^c(\tilde{x}_i) \neq \arg \max_c y_i^c$  then
         $A_t \leftarrow A_t \cup \{(x_i, y_i)\}$ 
      end if
    end for
     $\theta \leftarrow \theta - \eta \cdot \frac{1}{m+m'} \sum_{i=1}^{m+m'} \nabla_\theta [\ell_{CE}(f_\theta(\tilde{x}_i), y_i) + \beta \ell_{KL}(f_\theta(\tilde{x}_i), y_i)]$ 
  end for
end for

```

Algorithm 3 GAIRAT with guided interpolation framework (GAIRAT-GIF)

Input: model f_θ , training dataset S , learning rate η , number of epochs T , original batch size m , interpolation batch size m' , number of batches M , perturbation bound ϵ , step size α , PGD step number K

Output: adversarially robust network f_θ

```
 $A_0 \leftarrow S$ 
for epoch  $t = 1, 2, \dots, T$  do
   $A_t = \emptyset$ 
  Compute interpolation set  $\bar{S}_t$  by  $A_{t-1}$  and Eq. (9)
  for mini-batch  $= 1, \dots, M$  do
    Randomly sample  $\{(x_i, y_i)\}_{i=1}^m$  from  $S$  and  $\{(x_i, y_i)\}_{i=m+1}^{m+m'}$  from  $\bar{S}_t$ 
    for  $i = 1, \dots, m + m'$  do in parallel
       $\tilde{x}_i \leftarrow x_i; \kappa(x_i, y_i) \leftarrow 0$ 
      for  $k = 1, \dots, K$  do
        if  $\tilde{x}$  is predicted correctly then
           $\kappa(x_i, y_i) \leftarrow \kappa(x_i, y_i) + 1$ 
        end if
         $\tilde{x}_i \leftarrow \Pi_{\mathcal{B}_\epsilon(x_i)}(\alpha \text{sign}(\nabla_{\tilde{x}_i} \ell(f_\theta(\tilde{x}_i), y_i)) + \tilde{x}_i)$ 
      end for
      Compute  $\omega(x_i, y_i)$  according to  $\kappa(x_i, y_i)$ 
      if  $i \leq m$  and  $\arg \max_c f_\theta^c(\tilde{x}_i) \neq \arg \max_c y_i^c$  then
         $A_t \leftarrow A_t \cup \{(x_i, y_i)\}$ 
      end if
    end for
     $\theta \leftarrow \theta - \eta \cdot \nabla_\theta \left\{ \sum_{i=1}^{m+m'} \frac{\omega(x_i, y_i)}{\sum_{j=1}^{m+m'} \omega(x_j, y_j)} \ell(f_\theta(\tilde{x}_i), y_i) \right\}$ 
  end for
end for
```

Algorithm 4 FastAT with guided interpolation framework (FastAT-GIF)

Input: model f_θ , training dataset S , learning rate η , number of epochs T , original batch size m , interpolation batch size m' , number of batches M , perturbation bound ϵ , step size α , PGD step number K

Output: adversarially robust network f_θ

```
 $A_0 \leftarrow S$ 
for epoch  $t = 1, 2, \dots, T$  do
   $A_t = \emptyset$ 
  Compute interpolation set  $\bar{S}_t$  by  $A_{t-1}$  and Eq. (9)
  for mini-batch  $= 1, \dots, M$  do
    Randomly sample  $\{(x_i, y_i)\}_{i=1}^m$  from  $S$  and  $\{(x_i, y_i)\}_{i=m+1}^{m+m'}$  from  $\bar{S}_t$ 
    for  $i = 1, \dots, m + m'$  do in parallel
       $\tilde{x}_i \leftarrow x_i + \mathcal{U}(-\epsilon, \epsilon)$ 
       $\tilde{x}_i \leftarrow \Pi_{\mathcal{B}_\epsilon(x_i)}(\alpha \text{sign}(\nabla_{\tilde{x}_i} \ell(f_\theta(\tilde{x}_i), y_i)) + \tilde{x}_i)$ 
      if  $i \leq m$  and  $\arg \max_c f_\theta^c(\tilde{x}_i) \neq \arg \max_c y_i^c$  then
         $A_t \leftarrow A_t \cup \{(x_i, y_i)\}$ 
      end if
    end for
     $\theta \leftarrow \theta - \eta \cdot \frac{1}{m+m'} \sum_{i=1}^{m+m'} \nabla_\theta \ell(f_\theta(\tilde{x}_i), y_i)$ 
  end for
end for
```

B Detailed Experimental Settings

B.1 Detailed Experimental Settings of Figure 1 and 2

In Figure 1, we train three models with AT, AT-mixup, and AT-GIF respectively. The settings for these models are the same as our default settings (described in Section 4), except these models do not involve the burn-in period. The training of AT-mixup is shown in Algorithm 5, and the training of AT-GIF is shown in Algorithm 1.

In Figure 2, we randomly select 1,600 data from 2 random classes (800 data for each class) from the CIFAR-10 dataset. We embed the data to 2-dimension with PCA Abdi and Williams (2010). Then, we train these 2D data on a small neural network with four fully connected layers (size 10–10–5–2) with AT, AT-mixup, and AT-GIF, respectively. We visualize the prediction confidences in the three lower panels.

Algorithm 5 Adversarial training with vanilla mixup (AT-mixup)

Input: model f_θ , training dataset S , learning rate η , number of epochs T , original batch size m , interpolation batch size m' , number of batches M , perturbation bound ϵ , step size α , PGD step number K

Output: adversarially robust network f_θ

```
 $A_0 \leftarrow S$ 
for epoch  $t = 1, 2, \dots, T$  do
   $A_t = \emptyset$ 
  Compute interpolation set  $\bar{S}_t$  by training dataset  $S$  and Eq. (6)
  for mini-batch  $= 1, \dots, M$  do
    Randomly sample  $\{(x_i, y_i)\}_{i=1}^m$  from  $S$ 
    for  $i = 1, \dots, m$  do in parallel
      Generate adversarial data  $\tilde{x}_i$  of  $x_i$  by Eq. (3)
    end for
    Randomly sample  $\{(x_i, y_i)\}_{i=m+1}^{m+m'}$  from  $\bar{S}_t$ 
    for  $i = m + 1, \dots, m + m'$  do in parallel
      Generate adversarial data  $\tilde{x}_i$  of  $x_i$  by Eq. (3)
    end for
     $\theta \leftarrow \theta - \eta \cdot \frac{1}{m+m'} \sum_{i=1}^{m+m'} \nabla_{\theta} \ell(f_{\theta}(\tilde{x}_i), y_i)$ 
  end for
end for
```

B.2 Detailed Description of the Datasets

In our experiments, all the models are trained on the CIFAR-10 Krizhevsky (2009) and the SVHN Netzer et al. (2011) dataset.

The CIFAR-10 dataset consists of 60,000 32x32 colour images in 10 classes, with 6,000 images per class. There are 50,000 training images and 10,000 test images.

SVHN is a real-world image dataset consists of 73,257 training data and 26,032 testing data in 10 classes. SVHN is obtained from house numbers in Google Street View images.

B.3 Detailed Settings of Baselines

For fair comparisons, our GIF-based methods (TRADES-GIF, GAIRAT-GIF, and FastAT-GIF) keep the same settings as their original versions (TRADES Zhang et al. (2019), GAIRAT Zhang et al. (2021a), FastAT Wong et al. (2020)). In TRADES and TRADES-GIF, we set KL loss weight $\beta = 6$, weight of Gaussian noise $\gamma = 0.001$, and training epoch $T = 75$. The initial learning rate $\eta = 0.1$ and divided by 10 at Epoch 37 and 56, respectively. In GAIRAT and GAIRAT-GIF, we set geometry-aware weight assignment function $\omega(x, y) = \frac{1 + \tanh(-1 + 5 \times (1 - 2 \times \kappa(x, y) / K))}{2}$ according to Zhang et al. (2021a).

C Additional Experiments

C.1 Auxiliary Experiment for Comparisons Between AT, AT-mixup, and AT-GIF

We conduct an auxiliary experiment to further compare the differences between AT, AT-mixup, and AT-GIF on ResNet-18 He et al. (2016). First, we pretrain three ResNet-18 models on the whole CIFAR-10 dataset with AT, AT-mixup, and AT-GIF, respectively. Second, we randomly select 2,000 testing data from 2 random classes (1,000 data for each class) from the CIFAR-10 dataset. Third, we compute the prediction confidences of these 2,000 data with the three pretrained model. Fourth, we embed these data to 2-dimension with PCA Abdi and Williams (2010). Last, we visualize these data according to their prediction confidence in Figure 4. The prediction confidences of the model trained with AT-mixup behaves linearly. AT-GIF alleviates the linear issue and behaves sharply.

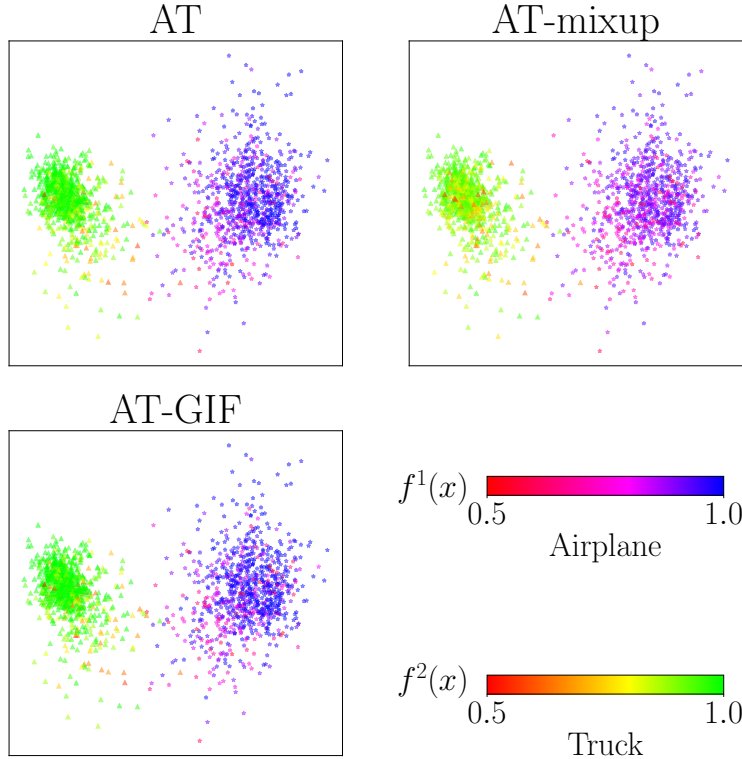


Figure 4: Comparisons between AT, AT-mixup, and AT-GIF on ResNet-18 He et al. (2016).

C.2 Robustness Evaluation of GIF Incorporating with Other AT methods on ResNet-18

We report the test accuracy of GIF incorporating with other AT methods on ResNet-18 in Table 7. The results show that all GIF-based methods outperform their original versions.

Table 7: Test accuracy of GIF incorporating with other AT methods on ResNet-18.

Defense	Network	Best				Last			
		Natural	PGD-20	CW	AA	Natural	PGD-20	CW	AA
TRADES	ResNet-18	81.28	52.05	49.63	48.53	81.17	51.81	49.35	48.41
TRADES-GIF		81.54	53.04	49.84	48.96	82.11	52.05	49.51	48.45
GAIRAT	ResNet-18	82.91	55.93	42.74	40.03	83.03	50.94	38.04	35.17
GAIRAT-GIF		81.29	60.57	43.07	40.36	81.07	60.08	40.09	37.43
Fast AT	ResNet-18	86.33	43.81	45.12	41.03	89.26	1.44	2.72	0.00
Fast AT-GIF		85.45	47.49	45.88	42.88	89.13	1.23	2.35	0.00

C.3 Robustness Evaluation of AT-GIF with Different Fixed Interpolation Weight λ

We report the test accuracy of AT-GIF with different fixed interpolation weight $\lambda \in \{0.1, 0.2, 0.3, 0.4, 0.5\}$. The results suggest that AT-GIF with $\lambda = 0.5$ achieves the best performance.

Table 8: Test accuracy of AT-GIF with different fixed interpolation weight λ .

Metric	AT-GIF (0.1)	AT-GIF (0.2)	AT-GIF (0.3)	AT-GIF (0.4)	AT-GIF (0.5)
Natural	84.42	84.10	83.73	83.46	81.59
PGD-20	47.88	49.72	52.27	52.81	53.57
CW	46.85	48.30	48.88	49.08	50.07

C.4 Robustness Evaluation of AT-GIF with Different Ratios of Original Data and Interpolated Data

We report the test accuracy of AT-GIF with different ratios of data from the original dataset and interpolation set on the CIFAR-10 dataset Krizhevsky (2009) in Table 9. The results suggest that GIF(1:1) is most effective for enhancing robustness.

Table 9: Test accuracy of AT-GIF with different ratios of original data and interpolated data on ResNet-18.

Defense	Natural	PGD-20	CW
AT-GIF (1:1)	81.59	53.57	50.07
AT-GIF (1:2)	81.90	53.05	49.33
AT-GIF (2:1)	82.88	51.98	49.47